

Impact of absorbing aerosol deposition on snow albedo reduction over the southern Tibetan plateau based on satellite observations

Wei-Liang Lee¹ · K. N. Liou² · Cenlin He² · Hsin-Chien Liang¹ · Tai-Chi Wang³ · Qinbin Li² · Zhenxin Liu² · Qing Yue²

Received: 30 January 2016 / Accepted: 25 June 2016
© Springer-Verlag Wien 2016

Abstract We investigate the snow albedo variation in spring over the southern Tibetan Plateau induced by the deposition of light-absorbing aerosols using remote sensing data from moderate resolution imaging spectroradiometer (MODIS) aboard Terra satellite during 2001–2012. We have selected pixels with 100 % snow cover for the entire period in March and April to avoid albedo contamination by other types of land surfaces. A model simulation using GEOS-Chem shows that aerosol optical depth (AOD) is a good indicator for black carbon and dust deposition on snow over the southern Tibetan Plateau. The monthly means of satellite-retrieved land surface temperature (LST) and AOD over 100 % snow-covered pixels during the 12 years are used in multiple linear regression analysis to derive the empirical relationship between snow albedo and these variables. Along with the LST effect, AOD is shown to be an important factor contributing to snow albedo reduction. We illustrate through statistical analysis that a 1-K increase in LST and a 0.1 increase in AOD indicate decreases in snow albedo by 0.75 and 2.1 % in the southern Tibetan Plateau, corresponding to local shortwave radiative forcing of 1.5 and 4.2 W m⁻², respectively.

1 Introduction

The mighty Tibetan Plateau, with an average altitude of 4.7 km and an area of about 2.4 million km², is referred to as the third pole of the Earth due to its massive permanent glacier and snow fields. It profoundly influences atmospheric general circulation because of its uplift of large-scale flows and its insertion of heating with a confining lower boundary at high levels. Numerous papers have testified to the two unsolved problems imposed by the Tibetan Plateau in the understanding of regional and global climate and climate change: the surface radiative heating rates over complex topography (Liou et al. 2007; Lee et al. 2013) and the snow albedo feedback induced by light-absorbing aerosols, chiefly black carbon (BC) (Jacobson 2004; IPCC 2007; Ramanathan et al. 2007; Ming et al. 2008; Yasunari et al. 2010; Liou et al. 2011; Hadley and Kirchstetter 2012; Liou 2013; Liou et al. 2014; He et al. 2014b). The energy budget of the coupled atmosphere-land system could be significantly modulated by changes in snow albedo since a small reduction in snow reflectivity can substantially increase the surface absorption of solar fluxes, which leads to further reduction in snow albedo (Hansen and Nazarenko 2004). Moreover, the snowpack in the Tibetan Plateau is the primary origin points of the Yangtze, Mekong, Yarlung Tsangpo-Brahmaputra, Ganges, and Indus rivers, which are the major water sources in China, Indochina, and the India subcontinent.

The albedo of snow surface, defined as the ratio of the reflected solar flux with reference to the incoming solar flux, is controlled by intrinsic snow properties including grain size and light-absorbing impurities, as well as other extrinsic conditions such as snow depth and solar zenith angle (e.g., Warren and Wiscombe 1980; Flanner and Zender 2006). The evolution of snow grain sizes is primarily determined by temperature and snow aging. Impurities in snow generally result from

✉ Wei-Liang Lee
leelupin@gate.sinica.edu.tw

¹ Research Center for Environmental Changes, Academia Sinica, Taipei, Taiwan

² Department of Atmospheric and Oceanic Sciences, Joint Institute for Regional Earth System Science and Engineering, University of California, Los Angeles, CA, USA

³ Institute of Statistical Science, Academia Sinica, Taipei, Taiwan

the wet scavenging of light-absorbing aerosols associated with cloud formation and precipitation processes. Both dry and wet deposition can reduce snow albedo and result in stronger absorption of solar radiation at the land surface, leading to a higher land surface temperature (LST) and consequently, faster snowmelt (Warren and Wiscombe 1980; Chylek et al. 1983; Ramanathan and Carmichael 2008).

Lee and Liou (2012) investigated the effect of light-absorbing aerosols on the reduction in snow albedo over the Sierra Nevada in spring utilizing snow albedo in 100 % snow-covered area (PSA), LST, and aerosol optical depth (AOD) data derived from moderate resolution imaging spectroradiometer (MODIS) onboard the NASA Terra satellite in March and April 2000–2009, as well as the precipitation data available from the NOAA Climate Prediction Center. Using multiple regression analysis, they demonstrated that AOD, which includes BC and dust over the Sierras transported from Asia and local emission, is an important factor to changes in snow albedo, second only to LST, while the impact of snowfall occurrence is insignificant.

Although the impact of aerosol deposition on the reduction of snow reflectivity is clear from ground measurement (e.g., Aoki et al. 2003), Warren (2013) indicated that it could be very difficult to evaluate its impact from the aspect of satellite remote sensing. Based on the radiative transfer calculation given by Warren and Wiscombe (1980), the difference in optical properties between snow with and without mixing of BC is too small to be detected by satellites for a given scene at a given time. However, this small snow albedo reduction due to mixing with BC could absorb more solar radiation and subsequently accelerate the growth of snow grains and snowmelt. Over a sufficiently long period of time (e.g., a month), it appears to be physically appropriate to postulate that snow albedo reduction caused by this nonlinear amplification effect can be detected on the basis of satellite retrievals. In addition, snow albedo can also be decreased by mixing with dust or direct dust deposition onto the snow surface. Therefore, this study seeks to use monthly mean remote sensing data to quantify the impact of aerosol deposition on snow albedo reduction.

The amount of BC deposition over the southern Tibetan Plateau has been investigated using ice cores and in situ measurements (e.g., Menon et al. 2010; Ginot et al. 2014; Jacobi et al. 2015). For example, using a trajectory analysis, Ming et al. (2008) found that two pathways are responsible for the primary transport of aerosols to the Himalayas. Long-distance and high-elevation transport has been related to westerlies from Central Asia which dominates in the non-monsoon season, while short-distance and low-elevation transport is largely modulated by the Indian summer monsoon. Employing the GEOS-Chem adjoint model (Henze et al. 2007), Kopacz et al. (2011) found that despite significant seasonal and geographical variability, emissions from India, Nepal, and China are the

major sources of BC over the southern Tibetan Plateau. In recent years, an increasing trend in BC emissions in South and Central Asia has been noted (Bond et al. 2007; Ramanathan et al. 2007). Most of the transport and circulation studies reveal that the deposition of light-absorbing aerosols, particularly BC, takes place in the southern part of the Tibetan Plateau, especially over the southern slope of the Himalayas (e.g., Ming et al. 2008; Lu et al. 2012). Moreover, mineral dust has been shown to be an important contributor to AOD in the Himalayas based on satellite remote sensing (Gautam et al. 2013). Ice core records also reveal that dust deposition is significant (Ginot et al. 2014). Dust is not as absorptive as BC, but the amount of dust deposition is much larger and could effectively reduce snow albedo. For this reason, we specifically investigate the potential correlation between PSA and aerosol deposition, including both BC and dust, in this region.

Accordingly, we have organized the paper as follows. In Section 2, we describe the observational data used in the study, including PSA, LST, and AOD, from the MODIS remote sensing products, as well as the precipitation data from Global Precipitation Climatology Project (GPCP) which is used to quantify the effect of snow aging. In Section 3, the GEOS-Chem simulation of BC and dust deposition during 2006–2008 is employed to validate the usage of MODIS-retrieved AOD as an index of light-absorbing aerosol deposition. The monthly averaged time series of PSA, LST, AOD, and snow aging effect over the southern Tibetan Plateau in March and April during 2001–2012 are presented in Section 4, where we have further discussed the application of multiple regression analysis to available datasets to evaluate the impact of light-absorbing aerosol deposition on the reduction in snow albedo. Concluding remarks are given in Section 5.

2 Data

Figure 1 is the elevation map of the Tibetan Plateau using GTOPO30 topography data at a 1-km resolution from the Earth Resources Observation and Science (EROS) data center of the US Geological Survey (USGS) National Center (<https://lta.cr.usgs.gov/GTOPO30>). The selection of the study area follows the definition of Hindu Kush–Karakorum–Himalaya mountain chain given by the Global Land Cover Network (GLCN) under the Food and Agriculture Organization (FAO) of the United Nations. Figure 1 also shows the 12-year mean of snow cover in March from 2001 to 2012 at a resolution of 500 m from MODIS dataset, when snow cover reaches its maximum of the year. It can be found that regions with snow cover larger than 90 % are generally located along the Hindu Kush–Karakorum–Himalaya mountain chain and the Pamir, while only limited and scattered snow-covered areas are observed

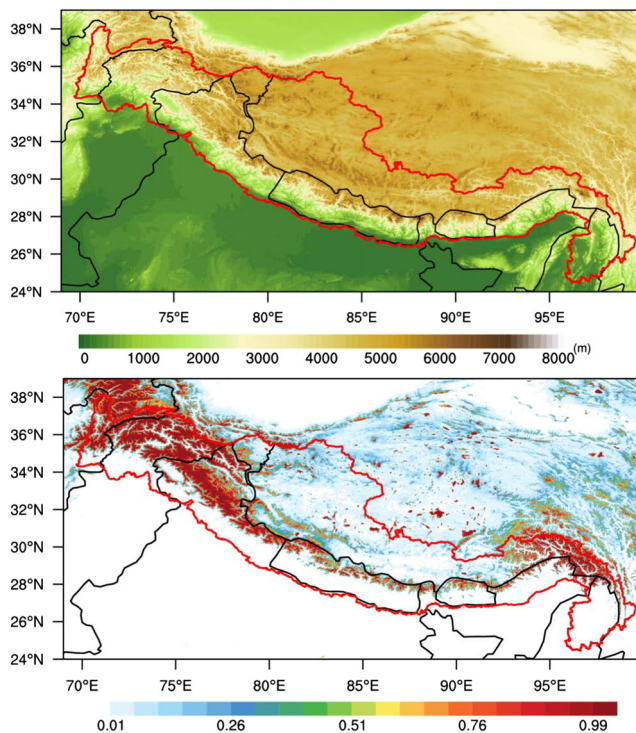


Fig. 1 Elevation map in the Tibetan Plateau region at a spatial resolution of 1 km (*top panel*) and 12-year mean of snow cover in March from 2001 to 2012 at a resolution of 500 m from MODIS remote sensing data (*bottom panel*). The *red curve* depicts the study area covering the Hindu Kush-Karakorum-Himalaya mountain chain defined by the Global Land Cover Network of United Nations

over the inland of the Tibetan Plateau. Therefore, the impact of snow albedo reduction should be the largest along the mountain chain, as demonstrated by Ménégos et al. (2014) and Kaspari et al. (2014).

From MODIS/Terra products, the daily fractional snow cover and broadband (visible and near-IR) snow albedo datasets are available at a 500-m resolution (Riggs et al. 2006), while the daily LST is available at a 1-km resolution (Wan 2012). The snow cover over the Tibetan Plateau has been validated with an accuracy of more than 90 %, as shown in the work of Pu et al. (2007). The algorithm of broadband snow albedo for the entire solar spectrum utilizes a look-up table approach in which the bidirectional reflectance distribution function (BRDF) of the snow fields was modeled by the discrete ordinates radiative transfer program (DISORT) (Stamnes et al. 1988). The local slope and aspect are also taken into account in this algorithm for snow albedo retrievals over mountains. The MODIS daily snow albedo over Greenland has been evaluated in Stroeve et al. (2006). They found that the correlation between MODIS retrievals and in situ observations can reach 0.79. Following Lee and Liou (2012), our objective is to document variation in snow albedo for pixels with fractional snow cover equal to unity (denoted as PSA) in March and April from 2001 to 2012 in order to avoid the contamination of snow albedo by other types of land

surfaces. It is noted that the atmospheric correction scheme for snow albedo retrieval assumes an AOD value of 0.05. Over the aerosol-laden Himalayas, it could result in underestimation of snow albedo. In addition, if the snow depth is very thin, the underlying ground can be exposed so that snow albedo could be underestimated. Using the snow depth analysis data from the Canadian Meteorological Centre (Brown and Brasnett 2010), we found that the snow depth for pixels with 100 % snow cover is generally more than 100 cm, indicating that this bias should be minimal.

The Level-3 AOD (0.55 μm wavelength) algorithm for MODIS/Terra was developed by Levy et al. (2007) for dark surfaces and by Hsu et al. (2004) for bright surfaces such as deserts and urban areas. The daily AOD data at a $1^\circ \times 1^\circ$ resolution contain many missing data because of clouds. To obtain a reliable monthly mean, only the pixels with more than ten valid values of daily AOD in the whole month are used in calculation. It should be noted that AOD cannot be measured if the field of view (FOV) is snow covered. Therefore, the Level-3 AOD is the mean of AOD for snow-free FOVs within a $1^\circ \times 1^\circ$ box. In this study, we assume that spatial variation in the concentration of floating aerosols in a 1-degree box is small enough so that the mean of AOD for snow-free FOVs is not very different from the real AOD mean over the grid box. The Level-3 MODIS AOD has been validated by Ruiz-Arias et al. (2013) who showed that in Central Asia, including the Tibetan Plateau, the correlation coefficient between the MODIS AOD and in situ AERONET measurement is 0.63, while the mean bias is 0.04, about 22 % of the climatology AOD average value of 0.19. Figure 2 depicts the spatial distributions of PSA, LST, and AOD corresponding to 100 % snow-covered pixels for March and April 2006.

To evaluate the effect of snow aging on snow albedo reduction, we employed GPCP 1-Degree Daily (1DD) precipitation dataset (Huffman et al. 2001). When precipitation is larger than 0.1 mm/day and LST is lower than 0°C , it is considered as a snowfall event. We also used the variable DAS (days after each snowfall event) introduced by Lee and Liou (2012) to represent the age of snow on the surface. DAS is defined as zero for the day with snowfall and increases by one for each following day without snowfall.

3 Relation between AOD and deposition of absorbing aerosols

Previous studies have found that the mixing of both BC and dust particles with snow grains can substantially reduce snow albedo, although of the two, BC is more effective due to its inherent optical properties (Liou et al. 2011). Based on the ice core record of BC deposition during the last 50 years in the Himalayas and using backward air trajectory analysis, Ming et al. (2008) illustrated that the

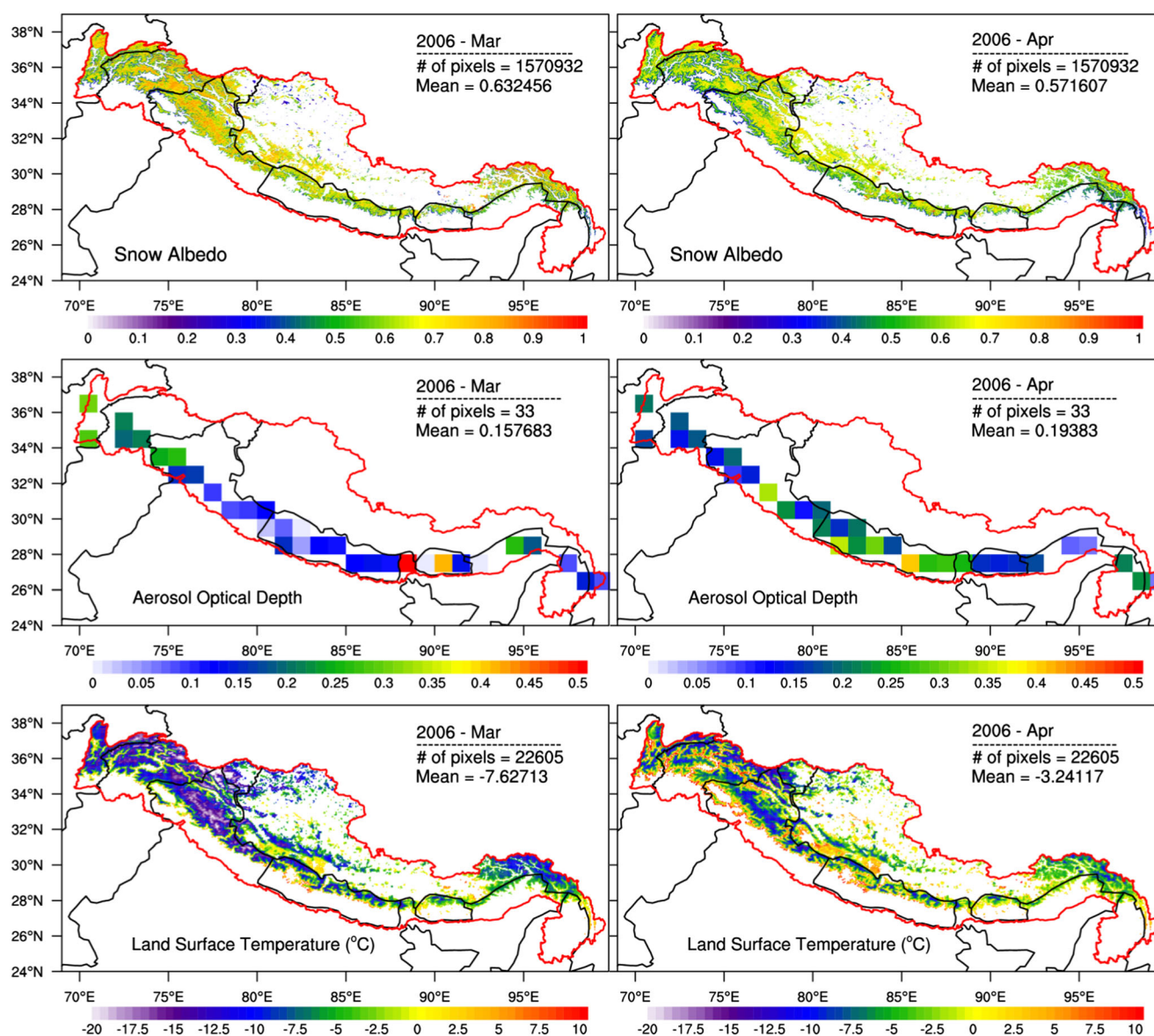


Fig. 2 Maps of the snow albedo, aerosol optical depth, and land surface temperature for pixels with 100 % snow cover for March and April 2006 from MODIS remote sensing data

BC emissions in South and Central Asia have significant effects on the BC deposit in the Himalayas. Moreover, these authors have estimated atmospheric BC concentrations based on the correlation equation developed by Davidson et al. (1993) in the form

$$C_a = \rho_a \times C_s / \omega, \quad (1)$$

where C_a is the aerosol concentration (ng m^{-3}) in the atmosphere, ρ_a is the air density (g m^{-3}), C_s is the aerosol concentration (ng g^{-1}) in snow, and ω is the scavenging ratio for a specific aerosol by snow falls. In view of this analysis, it appears evident that the deposition of light-absorbing aerosols onto the snow fields can be directly related to aerosol loading in the atmosphere.

To further examine the relationship between AOD and BC and dust deposition, including wet and dry deposition, we employed GEOS-Chem model (version 9-01-03) at a spatial resolution of $2^\circ \times 2.5^\circ$ with the meteorological fields given by the Goddard Earth Observing System (GEOS-5) of the NASA Global Modeling and Assimilation Office (GMAO). The global anthropogenic BC emission data was taken from Bond et al. (2007). However, the emission data in China and India were taken from Lu et al. (2011), since these two areas, which show a significant increase in BC emissions in recent years, are major source regions for BC transported to the Tibetan Plateau. For the rest of Asia, we used the data provided by Zhang et al. (2009). Global biomass burning emissions were based on the updated Global Fire Emissions Database version 3 (GFED3; van der Werf et al. (2010), Randerson et al.

(2012)). Additionally, we have used the global dust emission data provided in Zhang et al. (2013). For the dry deposition of aerosols in GEOS-Chem, a constant deposition velocity of 0.03 cm/s was prescribed over ice and snow (Wang et al. 2011), while the standard resistance-in-series scheme was used for other land types (Wesely 1989). The wet deposition scheme for aerosols was developed by Liu et al. (2001) and further updated by Wang et al. (2011). In this empirical scheme, the below-cloud scavenging including aerosol removal by snow and rain is formulated as $F = 1 - \exp(-k\Delta t)$, where F is the fraction of aerosols scavenged, Δt is the time step, and k is a first-order scavenging rate varying as a power of precipitation rate with different exponents for aerosols with accumulation/coarse modes removed by rain/snow. For in-cloud scavenging, all hydrophilic aerosols are removed in liquid and mix-phase clouds, while only dust and hydrophobic BC are removed in ice clouds. AOD in GEOS-Chem is calculated using the simulated aerosol concentration with prescribed aerosol optical properties derived from the Mie theory under various conditions such as aerosol sizes and relative humidity.

We have carried out a 3-year GEOS-Chem simulation from 2006 to 2008 (Zhang et al. 2013; He et al. 2014a) to calculate the monthly means of BC and dust deposition and AOD for March and April over the Himalayas. The mean AOD in this period is 0.119, and the contributions from BC, dust, sulfate, organic carbon, and sea salt are 0.005, 0.023, 0.065, 0.025, and 0.0006, respectively. As shown in Fig. 3, pixels with large BC and dust deposition are generally located in the southeastern part of the Himalayas, with a maximum occurring in April. The ratios of dry to wet deposition over the Himalayas are 0.12 for dust and 0.08 for BC, which are comparable to the values given in Jacobson (2004). The higher BC deposition in April than in March is caused by the following events. First, BC emissions from the biomass burning in India are higher in April, which are transported to the Himalayas by the valley wind (Bonasoni et al. 2010; Marinoni et al. 2013). The valley wind is stronger in April due to higher solar insolation, bringing more pollutants to high-altitude areas. Second, the stronger precipitation in April in this region implies higher wet deposition. In contrast, the BC deposition is almost zero over the inland of the Tibetan Plateau, probably because only a very small amount of BC originating in the Indian subcontinent and central China could be transported over high mountains (Lu et al. 2012). It is also found that dust is primarily transported from the Sahara desert (Zhang et al. 2013).

To establish the relation between AOD and the aerosol deposition in GEOS-Chem, we compute their correlation using AOD and the deposition in each pixel as the sample. We would like to point out that using both modeled AOD and modeled deposition for the analysis is more consistent, because the observed AOD in the real atmosphere could be affected by many complex processes such as subscale

aerosol-cloud interaction, which cannot be completely captured by the model. Thus, using MODIS AOD and modeled deposition may introduce a large uncertainty (or noise) in the analysis due to inconsistency in the two datasets (i.e., model and observation). Moreover, the model can capture all major processes in aerosol life cycles occurring in the real atmosphere, such as emission, transport, and deposition. Therefore, we analyzed the correlation between GEOS-Chem simulated AOD and BC/dust deposition and postulated that the relation is approximately correct as in the real atmosphere. It is found that the spatial distribution of AOD is similar to that of BC and dust deposition with correlation coefficients of 0.51 and 0.50, respectively, which are both significant at the 99 % level. It indicates that AOD can serve as a reasonable index for deposition of light-absorbing aerosols in the southern Tibetan Plateau. However, we note that the correlation analysis of AOD and BC/dust deposition could involve uncertainties, because a part of BC particles over a snow region could be transported by clouds from upwind regions, which form precipitation. Additionally, atmospheric aerosols contributing to AOD in this region may not deposit locally. Also, a part of AOD is contributed by non-absorbing sulfate particles, which do not affect snow reflectivity. It appears that these are possible reasons why correlation coefficients are not very strong. In order to reduce this type of uncertainty in satellite-based regression analysis, we have used spatial averages of the observed snow albedo, LST, and AOD over the entire Himalayas as input variables.

4 Analysis and discussion

The variables used for analysis, including PSA, LST, AOD, and DAS, are averaged to obtain monthly means for each selected pixel, followed by spatial averages to determine the mean value for all pixels within the study area. In this manner, 24 data points for each variable were obtained in March and April during 2001–2012. It should be noted that aerosols deposited in a specific grid over the Himalayas may come from upwind grids, while aerosols floating in a specific grid in the Himalayas, as represented by AOD, may also deposit in downwind grids. On the other hand, however, precipitation over the Tibetan Plateau and the northern Indian subcontinent during March and April primarily occurs along the Himalayas. It appears reasonable to argue that the majority of BC and dust depositions must be within this region. Therefore, we have used spatial means of input variables over the entire Himalayan region rather than individual grids for regression analysis for the specific purpose of reducing the abovementioned uncertainty. As illustrated in Fig. 4, PSA in the Himalayan region generally decreases from March to April because of higher LST and fewer snowfall events in April. PSA in March is at its lowest value in 2004, which

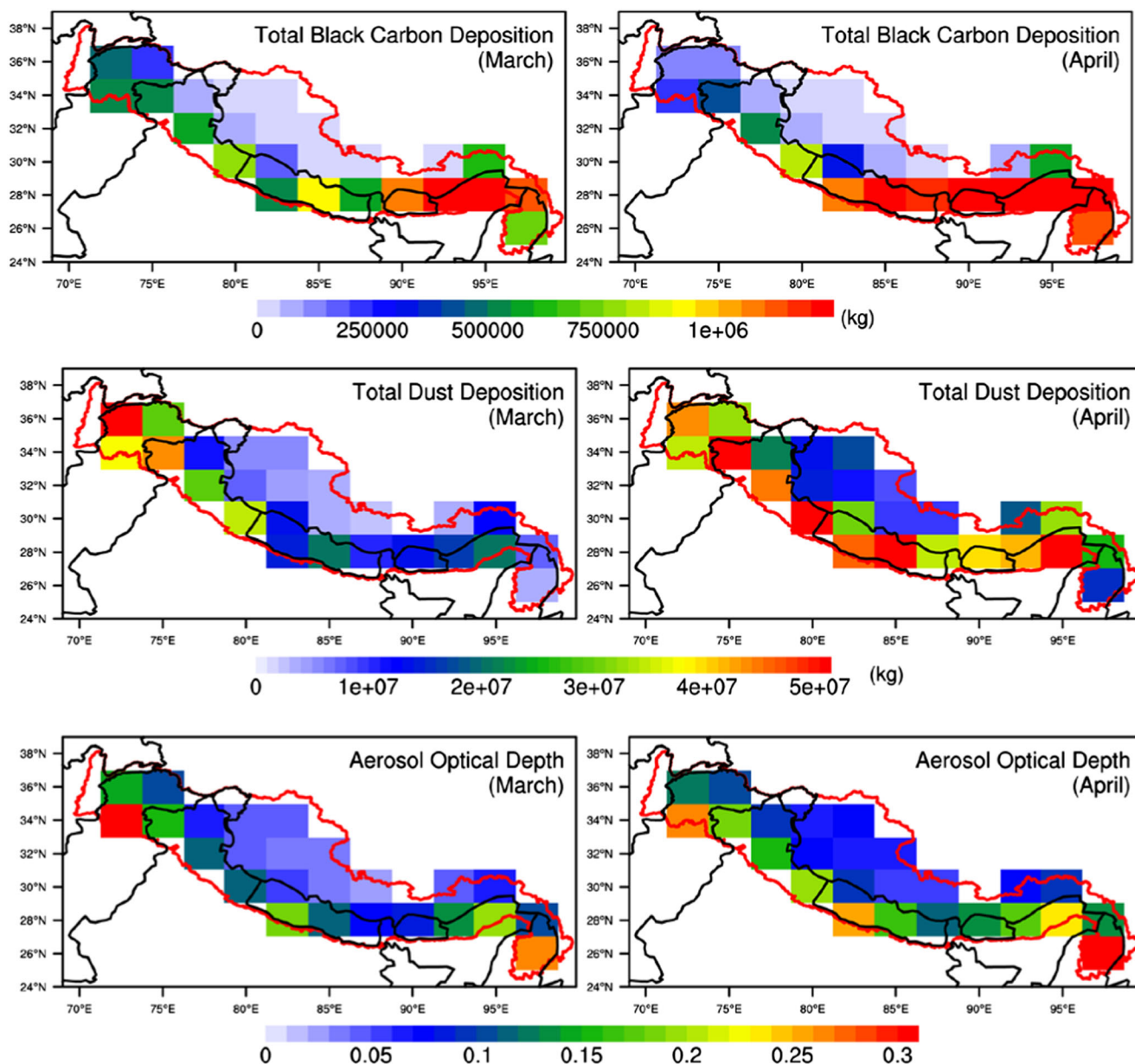


Fig. 3 Three-year means of the total black carbon deposition, total dust deposition, and aerosol optical depth simulated by GEOS-Chem for March and April of year 2006–2008

corresponds to maximum values of LST and DAS during the same period. In contrast, AOD has a strong interannual variation in springtime, as shown in Fig. 4c. Before 2007, AOD in March is generally smaller or almost equal to that in April, consistent with in situ observations in northern India during 2001–2006 (Lau et al. 2009). After 2008, we see substantial fluctuations of AOD, which could be larger in March than in April in certain years.

The correlations between PSA and the other three variables were also calculated using monthly mean data. As shown in Fig. 5, PSA has the largest correlation coefficient of -0.70 with LST, followed by -0.56 for DAS, and -0.40 for AOD, implying that LST and DAS have a greater impact on PSA

than AOD. The slopes of the regression lines in Fig. 5 are -0.0081 K^{-1} , -0.29 , and -0.046 day^{-1} for LST, AOD, and DAS, respectively. It is found that the correlation coefficient between LST and DAS is 0.9, while the correlations of AOD-LST and AOD-DAS pairs are both less than 0.2, revealing that it is appropriate to perform multiple linear regression using LST and AOD. However, it should be noted that these variables are not orthogonal. For example, more aerosols could increase cloud lifetime and consequently reduce downward solar radiation and LST. This aerosol indirect effect also leads to a larger DAS due to less precipitation. Moreover, the semi-indirect effects of light-absorbing aerosols could burn off clouds (Ten Hoeve et al. 2012), which increases downward

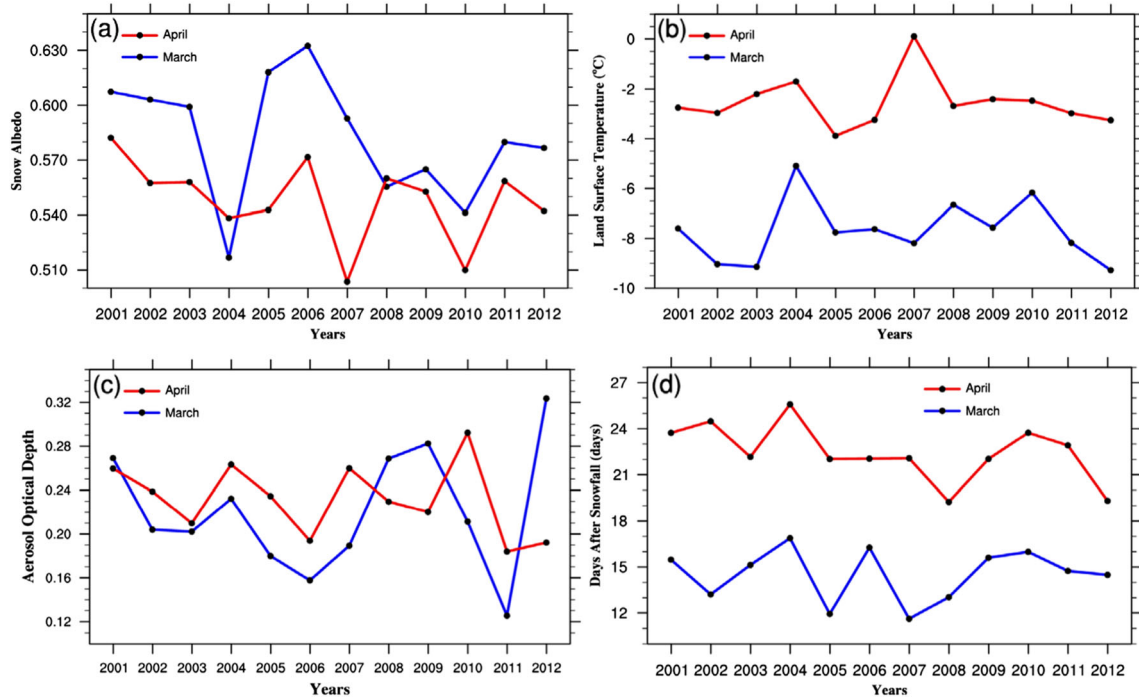


Fig. 4 Monthly averages of **a** snow albedo with 100 % snow cover (PSA), **b** land surface temperature (LST), **c** aerosol optical depth (AOD), and **d** days after snowfall (DAS) over the study area in March and April during 2001–2012

solar radiation and thus LST. Given the reasons above, we have utilized multiple linear regression to further evaluate the impacts of LST, DAS, and AOD on PSA. In addition, to represent the potential impact of seasonal changes in other meteorological parameters on snow albedo between March and April (e.g., humidity, wind speed, and wind direction), an indicator function I , which is equal to zero in March and one in April, is used in regression analysis. As a result, PSA can be predicted by

$$a = 0.499 - 0.015 \times LST + 0.0001 \times DAS - 0.19 \times AOD + 0.04I, \tag{2}$$

where a is the predicted PSA and the units of LST and DAS are defined by °C and days, respectively. The multiple

correlation coefficient (R^2) of this regression equation is 0.64 with a root mean square error (RMSE) of 0.022. The regression coefficient of DAS is positive, leading to an unrealistic inference that fewer snowy days could cause brighter snow. However, more detailed analysis reveals that the regression coefficient for DAS is not significantly different from zero. Since DAS is well correlated with LST as shown previously, the contribution of snow aging to snow albedo appears to be indirect when land surface temperature is taken into account, consistent with the results presented by Lee and Liou (2012). Moreover, it is also found that the correlation coefficient between LST and I is more than 0.92, implying that most seasonal changes related to snow albedo variation can be explained by LST. As a result, this indicator function is not necessary in the regression equation.

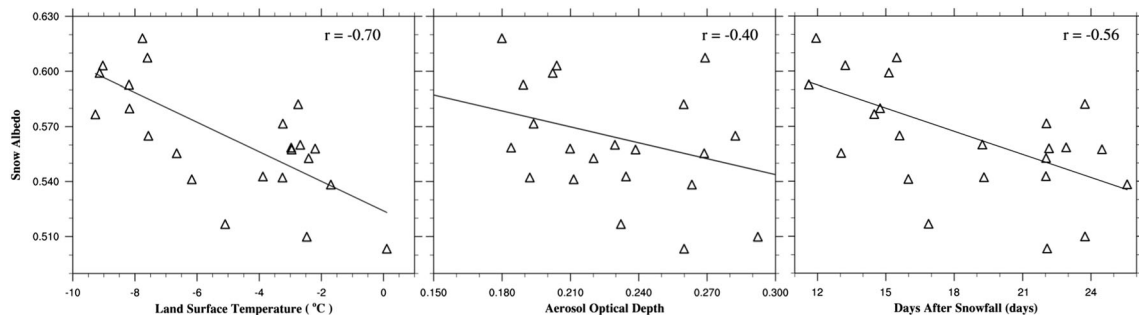


Fig. 5 Regression of snow albedo against land surface temperature, aerosol optical depth, and days after snowfall, with the correlation coefficients (r) also shown

For this reason, we have excluded DAS and I in the development of regression analysis such that PSA can be predicted by LST and AOD given by

$$a = 0.574 - 0.0075 \times LST - 0.21 \times AOD. \quad (3)$$

In this equation, R^2 is 0.57 with an RMSE of 0.021, and the relative differences between the real and predicted PSAs are within 10 %, as shown in Fig. 6. The standard deviations of the regression coefficients for LST and AOD are 0.0017 and 0.1049, respectively, with p values of 0.002 and 0.059. The 95 % confidence intervals are $-0.011 < LST < -0.004$ and $-0.43 < AOD < 0.009$. Equation 3 illustrates that if LST increases by 1 K, PSA will be reduced by 0.0075. Given that the climatological mean downward solar flux is about 200 W m^{-2} over the Tibetan Plateau, this PSA reduction corresponds to a shortwave radiative forcing of 1.5 W m^{-2} in this area. Similarly, a 0.1 increase in AOD leads to a 0.021 decrease in PSA, equivalent to a local shortwave radiative forcing of 4.2 W m^{-2} . For example, AOD drops by about 0.13 from March to April in 2012, and it could cause an increase in PSA by 0.027 and a radiative forcing of -5.5 W m^{-2} . The preceding discussion does not imply that AOD has a stronger impact on PSA than LST. To evaluate the relative importance of LST and AOD, both variables are first subtracted by their mean ($-5.11 \text{ }^\circ\text{C}$ for LST and 0.226 for AOD) and then divided by their standard deviations ($2.86 \text{ }^\circ\text{C}$ for LST and 0.0459 for AOD). The regression equation can now be expressed by:

$$a = 0.565 - 0.021T - 0.0096\tau, \quad (4)$$

where T and τ are standardized LST and AOD, respectively. The 95 % confidence intervals are $-0.031 < T < -0.011$ and $-0.020 < \tau < 0.0004$. Equation 4 predicts that a one standard

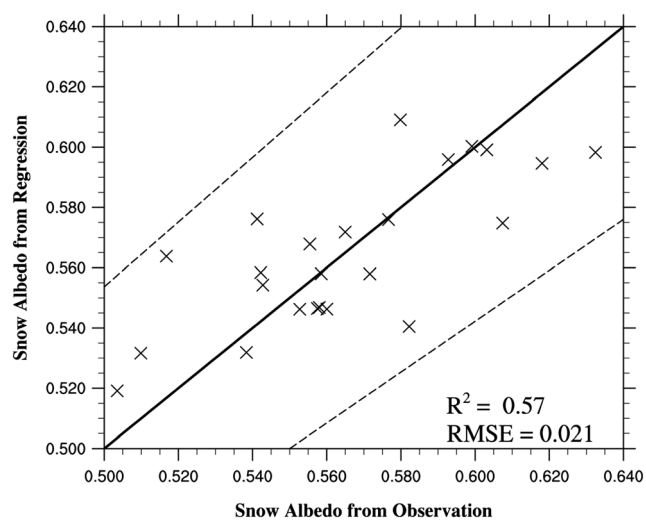


Fig. 6 Comparison of the snow albedo retrieved from satellite remote sensing and that predicted by the regression equation using land surface temperature and aerosol optical depth as input variables. Dash lines display a 10 % relative difference

deviation increase in LST and AOD would result in a 0.021 and 0.0096 reduction in PSA, respectively, implying that the impact of LST on PSA is about a factor of two larger than that of AOD.

We have also conducted another regression analysis using gridded data of PSA, LST, and AOD after all data are re-gridded to 1×1 -degree resolution. The R^2 of this regression equation is much smaller than that of Eq. 3. In addition, the regression coefficient of AOD does not significantly differ from zero, leaving LST the only variable determining PSA. This result echoes our previous argument that the floating aerosols in a specific grid box, as represented by AOD, may not deposit in the same grid.

The observed correlation found in this study does not necessarily prove the causal relationship between AOD and snow albedo reduction. Nevertheless, the correlation, albeit statistical, does imply a degree of the impact of light-absorbing aerosol deposition on snow albedo reduction. To physically understand causality or mechanism would require sensitivity analysis using a credible coupled atmosphere-land surface model that includes chemical transport, cloud microphysics, and radiative transfer, a challenging task requiring future work.

5 Concluding remarks

We have investigated the effect of AOD, which is correlated with the deposition of light-absorbing aerosols on snow, on snow albedo reduction over the southern Tibetan Plateau in March and April from 2001 to 2012. Remote sensing data used in the analysis, which includes snow cover, snow albedo, LST, and AOD, were obtained from the MODIS/Terra satellite. The daily GPCP precipitation data, together with LST, are used to identify snowfall events. The impact of snow aging is represented by DAS. We have selected only the pixels with 100 % snow cover to remove the effect of other types of land surface on snow albedo evaluation.

We have used the GEOS-Chem simulation for 2006–2008 to investigate the relationship between AOD and deposition of BC and dust, which can effectively reduce the reflectivity of snow grains. We showed that the correlation coefficients between the monthly averaged AOD and BC deposition and between AOD and dust deposition are 0.51 and 0.50, respectively, over the southern Tibetan Plateau for March and April, which are significant at the 0.01 level. Therefore, the satellite-retrieved AOD can be used as an appropriate index to evaluate the impact of aerosol deposition on snow albedo reduction in this region.

Employing multiple linear regression, snow albedo for pixels with 100 % snow cover (PSA) can be expressed as a function of LST, AOD, and DAS. The present results show that the impact of DAS on PSA is insignificant. Since DAS is highly correlated with LST, the snow aging effect is rather indirect and closely related to surface temperature. The

regression model using LST and AOD as input variables can explain 57 % of the variation in PSA. If both LST and AOD vary by one standard deviation, the magnitude of the impact of LST is about two times larger than that of AOD. As shown by this empirical regression model, when LST increases by 1 K, the snow albedo in the southern Tibetan Plateau will decrease by 0.75 %, equivalent to a shortwave radiative forcing of 1.5 W m^{-2} over this region. Correspondingly, a 0.1 increase in AOD will lead to a 2.1 % decrease in snow albedo, equivalent to a 4.2 W m^{-2} solar radiative forcing. While this statistical study may not prove the cause-and-effect relationship between AOD and snow albedo, it appears that the present data analysis could provide a quantitative basis for model development and simulations involving more detailed physical processes of aerosols and snow. For example, the regression coefficient of LST in Eq. 3 is smaller than the slope shown in Fig. 5. It should be noted that the impact of AOD on PSA is included in the simple PSA-LST regression using observation data. Therefore, the sensitivity of PSA to LST is in fact smaller, and it should be considered in model development and tuning.

Acknowledgments This research is supported by the Ministry of Science and Technology of Taiwan under contract MOST 103-2111-M-001-007 and by the Department of Energy of the United States under Grant DESC0006742 and the National Science Foundation under Grant AGS-0946315. We thank NASA's Earth Observing System Data and Information System (EOSDIS) for providing MODIS/Terra retrievals.

References

- Aoki T, Hachikubo A, Hori M (2003) Effects of snow physical parameters on shortwave broadband albedos. *J Geophys Res* 108(D19):4616. doi:10.1029/2003JD003506
- Bond TC, Bhardwaj E, Dong R, Jogani R, Jung S, Roden C, Streets DG, Trautmann NM (2007) Historical emissions of black and organic carbon aerosol from energy-related combustion, 1850–2000. *Glob Biogeochem Cycles* 21:GB2018
- Bonasoni P, Laj P, Marinoni A, Sprenger M, Angelini F, Arduini J, Bonae U, Calzolari F, Colombo T, Decesari S, Di Biagio C, di Sarra AG, Evangelisti F, Duchi R, Facchini C, Fuzzi S, Gobbi GP, Maione M, Panday A, Roccatto F, Sellegri K, Venzac H, Verza GP, Villani P, Vuillermoz E, Cristofanelli P (2010) Atmospheric Brown clouds in the Himalayas: first two years of continuous observations at the Nepal climate observatory-pyramid (5079 m). *Atmos Chem Phys* 10:7515–7531. doi:10.5194/acp-10-7515-2010
- Brown RD, Brasnett B (2010) Canadian Meteorological Centre (CMC) daily snow depth analysis data. Boulder, Colorado USA: NASA National Snow and Ice Data Center Distributed Active Archive Center. <http://dx.doi.org/10.5067/W9FOYWH0EQZ3>
- Chylek P, Ramaswamy V, Srivastava V (1983) Albedo of soot contaminated snow. *J Geophys Res* 88:10837–10843
- Davidson CI, Jaffrezo JL, Mosher BW, Dibb JE, Borys RD, Bodhaine BA, Rasmussen RA, Boutron CF, Ducroz FM, Cachier M, Ducret J, Collin JL, Heidam NZ, Kemp K, Hillamos R (1993) Chemical constituents in the air and snow at dye 4, Greenland: II. Analysis of episodes in April 1989. *Atmos Environ* 27(A):2723–2738
- Flanner MG, Zender CS (2006) Linking snowpack microphysics and albedo evolution. *J Geophys Res* 111:D12208. doi:10.1029/2005JD006834
- Gautam R, Hsu NC, Lau WK-M, Yasunari TJ (2013) Satellite observations of desert dust-induced Himalayan snow darkening. *Geophys Res Lett* 40:988–993. doi:10.1002/grl.50226
- Ginot P, Dumont M, Lim S, Patris N, Taupin J-D, Wagnon P, Gilbert A, Arnaud Y, Marinoni A, Bonasoni P, Laj P (2014) A 10 year record of black carbon and dust from a Mera peak ice core (Nepal): variability and potential impact on melting of Himalayan glaciers. *Cryosphere* 8:1479–1496. doi:10.5194/tc-8-1479-2014
- Hadley OL, Kirchstetter TW (2012) Black carbon snow albedo reduction. *Nat Clim Chang* 2:437–440
- Hansen J, Nazarenko L (2004) Soot climate forcing via snow and ice albedo. *Proc Natl Acad Sci U S A* 101:423–428. doi:10.1073/pnas.2237157100
- Henze DK, Hakami A, Seinfeld JH (2007) Development of the adjoint of GEOS-Chem. *Atmos Chem Phys* 7:2413–2433. doi:10.5194/acp-7-2413-2007
- He C, Li Q, Liou KN, Zhang J, Qi L, Mao Y, Gao M, Lu Z, Streets DG, Zhang Q, Sarin MM, Ram K (2014b) A global 3-D CTM evaluation of black carbon in the Tibetan Plateau. *Atmos Chem Phys* 14:7091–7112. doi:10.5194/acp-14-7091-2014
- He C, Li Q, Liou KN, Takano Y, Gu Y, Qi L, Mao Y, Leung LR (2014a) Black carbon radiative forcing over the Tibetan Plateau. *Geophys Res Lett* 41:7806–7813. doi:10.1002/2014GL062191
- Hsu NC, Tsay SC, King MD, Herman JR (2004) Aerosol properties over bright-reflecting source regions. *IEEE Trans Geosci Remote Sens* 42:557–569
- Huffman GJ, Adler RF, Morrissey M, Bolvin DT, Curtis S, Joyce R, McGavock B, Susskind J (2001) Global precipitation at one-degree daily resolution from multi-satellite observations. *J Hydrometeorol* 2:36–45
- Intergovernmental Panel on Climate Change (2007) Climate change 2007: the physical science basis. edited by Solomon S, Qin D, Manning M, Chen Z, Marquis M, Averyt K, Tignor M, Miller H. Cambridge University Press, Cambridge, UK, 996 pp.
- Jacobi H-W, Lim S, Ménégoz M, Ginot P, Laj P, Bonasoni P, Stocchi P, Marinoni A, Arnaud Y (2015) Black carbon in snow in the upper Himalayan Khumbu Valley, Nepal: observations and modeling of the impact on snow albedo, melting, and radiative forcing. *Cryosphere* 9:1685–1699. doi:10.5194/tc-9-1685-2015
- Jacobson MZ (2004) Climate response of fossil fuel and biofuel soot, accounting for soot's feedback to snow and sea ice albedo and emissivity. *J Geophys Res* 109:D21201. doi:10.1029/2004JD004945
- Kaspari S, Painter TH, Gysel M, Skiles SM, Schwikowski M (2014) Seasonal and elevational variations of black carbon and dust in snow and ice in the Solu-Khumbu, Nepal and estimated radiative forcings. *Atmos Chem Phys* 14:8089–8103. doi:10.5194/acp-14-8089-2014
- Kopacz M, Mauzerall DL, Wang J, Leibensperger EM, Henze DK, Singh K (2011) Origin and radiative forcing of black carbon transported to the Himalayas and Tibetan Plateau. *Atmos Chem Phys* 11:2837–2852. doi:10.5194/acp-11-2837-2011
- Lau WK, Kim K-M, Hsu N-YC, Holben BN (2009) Possible influences of air pollution, dust and sandstorms on the Indian monsoon. *WMO Bull* 58(1):22–30
- Lee W-L, Liou KN (2012) Effect of absorbing aerosols on snow albedo reduction in the sierra Nevada. *Atmos Environ* 55:425–430
- Lee W-L, Liou KN, Wang C-C (2013) Impact of 3-D topography on surface radiation budget over the Tibetan Plateau. *Theor Appl Climatol* 113:95–103. doi:10.1007/s00704-012-0767-y
- Levy RC, Remer LA, Mattoo S, Vermote EF, Kaufman YJ (2007) Second generation operational algorithm: retrieval of aerosol properties over land from inversion of moderate resolution imaging spectroradiometer spectral reflectance. *J Geophys Res* 112:D13211. doi:10.1029/2006JD007811

- Liou KN, Lee W-L, Hall A (2007) Radiative transfer in mountains: application to the Tibetan Plateau. *Geophys Res Lett* 34:L23809. doi:10.1029/2007GL031762
- Liou KN, Takano Y, Yang P (2011) Light absorption and scattering by aggregates: application to black carbon and snow grains. *J Quant Spectrosc Radiat Transf* 112:1581–1594
- Liou KN (2013) Radiative transfer and regional climate change. In “Radiative processes in the atmosphere and ocean (IRS2012)”. American Institute of Physics: pp. 35–38. doi:10.1063/1.40804701
- Liou KN, Takano Y, He C, Yang P, Leung RL, Gu Y, Lee W-L (2014) Stochastic parameterization for light absorption by internally mixed BC/dust in snow grains for application to climate models. *J Geophys Res* 119:7616–7632. doi:10.1002/2014JD021665
- Liu HY, Jacob DJ, Bey I, RM Y (2001) Constraints from Pb-210 and Be-7 on wet deposition and transport in a global three-dimensional chemical tracer model driven by assimilated meteorological fields. *J Geophys Res Atmos* 106:12109–12128. doi:10.1029/2000jd900839
- Lu Z, Zhang Q, Streets DG (2011) Sulfur dioxide and primary carbonaceous aerosol emissions in China and India, 1996–2010. *Atmos Chem Phys* 11:9839–9864. doi:10.5194/acp-11-9839-2011
- Lu Z, Streets DG, Zhang Q, Wang S (2012) A novel back-trajectory analysis of the origin of black carbon transported to the Himalayas and Tibetan Plateau during 1996–2010. *Geophys Res Lett* 39: L01809. doi:10.1029/2011GL049903
- Marinoni A, Cristofanelli P, Laj P, Duchi R, Putero D, Calzolari F, Landi TC, Vuillermoz E, Maione M, Bonasoni P (2013) High black carbon and ozone concentrations during pollution transport in the Himalayas: five years of continuous observations at NCO-P global GAW station. *J Environ Sci* 25:1618–1625. doi:10.1016/S1001-0742(12)60242-3
- Ménégoz M, Krinner G, Balkanski Y, Boucher O, Cozic A, Lim S, Ginot P, Laj P, Gallée H, Wagnon P, Marinoni A, Jacobi HW (2014) Snow cover sensitivity to black carbon deposition in the Himalayas: from atmospheric and ice core measurements to regional climate simulations. *Atmos Chem Phys* 14:4237–4249. doi:10.5194/acp-14-4237-2014
- Menon S, Koch D, Beig G, Sahu S, Fasullo J, Orlikowski D (2010) Black carbon aerosols and the third polar ice cap. *Atmos Chem Phys* 10: 4559–4571. doi:10.5194/acp-10-4559-2010
- Ming J, Cachier H, Xiao C, Qin D, Kang S, Hou S, Xu J (2008) Black carbon record based on a shallow Himalayan ice core and its climatic implications. *Atmos Chem Phys* 8:1343–1352
- Pu Z, Xu L, Salomonson VV (2007) MODIS/Terra observed seasonal variations of snow cover over the Tibetan Plateau. *Geophys Res Lett* 34:L0706
- Ramanathan V, Li F, Ramana M, Praveen PS, Kim D, Corrigan CE, Nguyen H, Stone EA, Schauer JJ, Carmichael GR, Adhikary B, Yoon SC (2007) Atmospheric brown clouds: hemispherical and regional variations in long range transport, absorption, and radiative forcing. *J Geophys Res* 112:D22S21
- Ramanathan V, Carmichael G (2008) Global and regional climate changes due to black carbon. *Nat Geosci* 1:221–227. doi:10.1038/ngeo156
- Randerson JT, Chen Y, van der Werf GR, Rogers BM, Morton DC (2012) Global burned area and biomass burning emissions from small fires. *J Geophys Res Biogeosci* 117:G04012. doi:10.1029/2012jg002128
- Riggs GA, Hall DK, Salomonson VV (2006) MODIS snow products user guide. <http://modis-snow-ice.gsfc.nasa.gov/sugkc2.html>
- Ruiz-Arias JA, Dudhia J, Gueymard CA, Pozo-Vázquez D (2013) Assessment of the Level-3 MODIS daily aerosol optical depth in the context of surface solar radiation and numerical weather modeling. *Atmos Chem Phys* 13:675–692. doi:10.5194/acp-13-675-2013
- Stamnes K, Tsay SC, Wiscombe W, Jayaweera K (1988) Numerically stable algorithm for discrete-ordinate-method radiative transfer in multiple scattering and emitting layered media. *Appl Opt* 27(12): 2502–2509. doi:10.1364/AO.27.002502
- Stroeve JC, Box J, Haran T (2006) Evaluation of the MODIS (MOD10A1) daily snow albedo product over the Greenland ice sheet. *Remote Sens Environ* 105(2):155–171. doi:10.1016/j.rse.2006.06.009
- Ten Hoeve JE, Jacobson MZ, Remer LA (2012) Comparing results from a physical model with satellite and in situ observations to determine whether biomass burning aerosols over the Amazon brighten or burn off clouds. *J Geophys Res* 117:D08203. doi:10.1029/2011JD016856
- van der Werf GR, Randerson JT, Giglio L, Collatz GJ, Mu M, Kasibhatla PS, Morton DC, DeFries RS, Jin Y, van Leeuwen TT (2010) Global fire emissions and the contribution of deforestation, savanna, forest, agricultural, and peat fires (1997–2009). *Atmos Chem Phys* 10: 11707–11735. doi:10.5194/acp-10-11707-2010
- Wan Z (2012) MODIS/Aqua Land Surface Temperature/Emissivity Daily L3 Global 0.05Deg CMG, 2000–2009. EDC LPDAAC, Sioux Falls, South Dakota, USA. Digital media.
- Wang Q, Jacob DJ, Fisher JA, Mao J, Leibensperger EM, Carouge CC, Le Sager P, Kondo Y, Jimenez JL, Cubison MJ, Doherty SJ (2011) Sources of carbonaceous aerosols and deposited black carbon in the Arctic in winter-spring: implications for radiative forcing. *Atmos Chem Phys* 11:12453–12473. doi:10.5194/acp-11-12453-2011
- Warren S, Wiscombe W (1980) A model for the spectral albedo of snow II: snow containing atmospheric aerosols. *J Atmos Sci* 37:2734–2745
- Warren SG (2013) Can black carbon in snow be detected by remote sensing? *J Geophys Res* 118:779–786. doi:10.1029/2012JD018476
- Wesely ML (1989) Parameterization of surface resistances to gaseous dry deposition in regional-scale numerical models. *Atmos Environ* 23: 1293–1304. doi:10.1016/0004-6981(89)90153-4
- Yasunari TJ, Bonasoni P, Laj P, Fujita K, Vuillermoz E, Marinoni A, Cristofanelli P, Duchi R, Tartari G, Lau K-M (2010) Estimated impact of black carbon deposition during pre-monsoon season from Nepal Climate Observatory—pyramid data and snow albedo changes over Himalayan glaciers. *Atmos Chem Phys* 10:6603–6615
- Zhang Q, Streets DG, Carmichael GR, He KB, Huo H, Kannari A, Klimont Z, Park IS, Reddy S, Fu JS, Chen D, Duan L, Lei Y, Wang LT, Yao ZL (2009) Asian emissions in 2006 for the NASA INTEX-B mission. *Atmos Chem Phys* 9:5131–5153
- Zhang L, Li QB, Gu Y, Liou KN, Meland B (2013) Dust vertical profile impact on global radiative forcing estimation using a coupled chemical-transport-radiative-transfer model. *Atmos Chem Phys* 13:7097–7114. doi:10.5194/acp-13-7097-2013